Lawrence Berkeley National Laboratory
LBL Publications

Authors
Young-Robertson, Jessica M
Raz-Yaseef, Naama
Cohen, Lily R
et al.
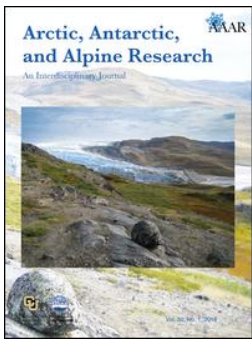
Evaporation dominates evapotranspiration on Alaska's Arctic Coastal Plain

Jessica M. Young-Robertson, Naama Raz-Yaseef, Lily R. Cohen, Brent Newman, Thom Rahn, Victoria Sloan, Cathy Wilson & Stan D. Wullschleger

Published online: 21 May 2018.

Submit your article to this journal

Article views: 203

View Crossmark data

Taylor & Francis
Taylor & Francis Group

Evaporation dominates evapotranspiration on Alaska's Arctic Coastal Plain

Jessica M. Young-Robertson[a], Naama Raz-Yaseef[b], Lily R. Cohen[c], Brent Newman[d], Thom Rahn[d], Victoria Sloan[e], Cathy Wilson[d], and Stan D. Wullschleger[f]

[a]School of Natural Resources and Extension, University of Alaska Fairbanks, Fairbanks, Alaska, USA; [b]Lawrence Berkley National Laboratory, Berkeley, California, USA; [c]International Arctic Research Center, University of Alaska Fairbanks, Fairbanks, Alaska, USA; [d]Los Alamos National Laboratory, Los Alamos, New Mexico, USA; [e]Department of Civil Engineering, University of Bristol, Bristol, UK; [f]Oak Ridge National Laboratory, Oak Ridge, Tennessee, USA

ABSTRACT

The dynamics of evapotranspiration (ET), such as the partitioning to evaporation and transpiration, of polygonal ground on the Arctic Coastal Plain are not well understood. We assessed ET dynamics, including evaporation and transpiration partitioning, created by microtopographic features associated with high- and low-centered polygons. Chamber ET and leaf-level transpiration measurements were conducted in one-week field campaigns in two growing seasons with contrasting weather conditions. We found that ET was greater in the drier and warmer sampling period (2013) compared to the colder and wetter one (2014). Evaporation dominated ET, particularly in the wetter and colder sampling period (>90% in 2014 vs. 80% in 2013). In the 2013 sampling period, wetter and warmer conditions increased ET and the contribution of transpiration to ET. If the soils warm with degrading permafrost, ET and the fraction contributed by transpiration may increase to a certain threshold, when moisture must increase with rising temperatures to further increase these fluxes. While the fraction of transpiration may rise with warmer soils, it is unlikely that transpiration will completely dominate ET. This work highlights the complexities of understanding ET in this dynamic environment and the importance of understanding differences across polygonal ground.

Introduction

Arctic landscapes characterized by low gradients in slope, such as the northern Alaska Arctic Coastal Plain, are vulnerable to the impacts of climate change on permafrost and hydrology (Hinzman et al. 2013). This is because even small changes in the subsurface morphology and surface microtopography can alter hydrology flowpaths (Liljedahl, Hinzman, and Schulla 2012), soil moisture (Engstrom et al. 2005), and soil thermal dynamics (Kane et al. 2000, 2008).

In the Arctic Coastal Plain, ice-wedge polygons are important geomorphic landforms with spatially variable soil moisture and temperature that relates to their shape. Polygons can have low, flat, or high centers relative to the rim (e.g., Ping et al. 1998). The centers of low-centered polygons typically have wet or saturated soil surrounded by unsaturated elevated rims, compared to the drier centers of high-centered polygons (Ping et al. 1998). Flooded or nearly saturated troughs occur between the polygons (Liljedahl et al. 2011; Olivas et al. 2011). As the polygons transition from low to high centered with degradation of the ice supporting the rim (Gamon et al. 2012; Jorgenson and Osterkamp 2005), the centers transition from wet to dry. However, not all high-centered polygons are degrading (e.g., Kanevskiy et al. 2013). Thus, degrading permafrost in polygonal ground can further increase the spatial variability in soil moisture and temperature (Engstrom et al. 2005; Gamon et al. 2012; Olivas et al. 2011). As polygons degrade, plant communities shift from being less species rich and dominated by sedges and mosses to being more species rich and dominated by rushes and shrubs (Wullschleger et al. 2014). Nonvascular plants also shift with ice-wedge degradation, as lichen dominate dry areas and mosses are found in wetter areas (Gamon et al. 2013). Such shifts may impact ecosystem-level processes such as evapotranspiration (ET) and potentially the partitioning between evaporation and transpiration.

Evapotranspiration dominates hydrological processes on the Arctic Coastal Plain for a couple of months after snowmelt until soil moisture declines (Kane, Gieck, and Hinzman 1990; Kane et al. 2008, 2000). The majority of studies on ET in the Arctic tundra focus on whole eco-system fluxes, with rates of approximately 1–3 mm day^{-1} (Dery et al. 2005; Engstrom et al. 2006; Liljedahl et al. 2011; Mendez, Hinzman, and Kane 1998). However, a whole-ecosystem approach to determining ET rates does not allow for quantifying the variability in fluxes associated with the heterogeneous landscape (Oren et al. 2006), particularly on the Arctic Coastal Plain (Oechel et al. 1998). Further, a whole-ecosystem approach does not allow for partitioning ET into its components of evaporation and transpiration. Spatial heterogeneity in soil moisture, soil temperature, and plant composition likely affect how ET is partitioned into evaporation and transpiration in the Arctic Coastal Plain (Oberbauer and Dawson 1992). It is critical to understand the partitioning of evapotranspiration because environmental processes control evaporation and transpiration differently (Jasechko et al. 2013). While both respond to surface energy, atmospheric demand, and soil water availability (Betts, Goulden, and Wofsy 1999; Calder 1998), evapora-tion is a physical process and transpiration is a plant physiological process controlled by stomata (Wullschleger, Meinzer, and Vertessy 1998).

The goal of this study is to assess ET dynamics, and, more specifically, to partition ET into evaporation and transpiration, for different microtopographies related to polygonal ground. We focus on a gradient in hydrology (dry to wet areas) caused by variation in permafrost geomorphology. We hypothesize that wet areas are dominated by evaporation to a greater extent than drier areas. In field campaigns, we measured ET with small chambers, leaf level transpiration, soil moisture and temperature, and meteorological variables. We uti-lized Bayesian statistics to quantify the differences in ET, evaporation, and transpiration between the differ-ent microtopographic positions.

Methods

Site description

The study sites are located in Utqiaġvik (formerly Barrow), Alaska, (71.3°N, 156.5°W), which lies within the Alaskan Arctic Coastal Plain (Figure 1). This study was performed within the Barrow Environmental Observatory (BEO), which is located approximately
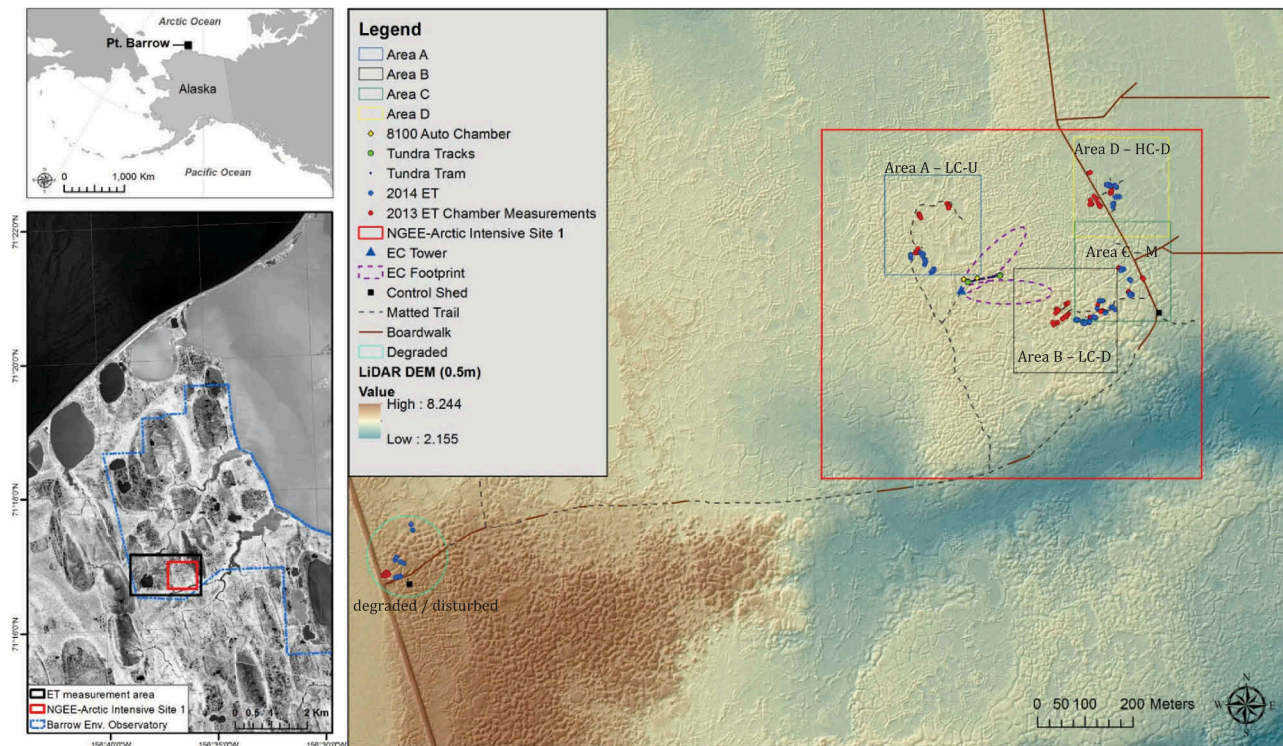
Figure 1. Map of the field study locations on the Alaskan Arctic Coastal Plain near Utqiaġvik (formerly Barrow), Alaska (71.3°N, 156.5°W). The areas are the following polygon types: area A is low-centered undegraded (LC-U), area B is low-centered degraded (LC-D), area C is mixed (M), area D is high-centered degraded (HC-D), and the degraded/disturbed area (turquoise-colored circle below the map legend) is characterized by multiple anthropogenic impacts, in addition to thermal degradation.

6 km east of Utqiaġvik. The permafrost is continuous and ice rich (Kanevskiy et al. 2013). Mean annual air temperature is $-12 \pm 4°C$ and mean annual precipitation is 180 ± 51 mm, with approximately half of the precipitation falling as rain during the short summer (1949–2014; Barrow W Post W Rogers Airport Meteorological Station, AK, USA).

Polygonal features dominate the land surface (Hubbard et al. 2013). For this study, five plots were identified to cover a variety of polygon types and degradation conditions (e.g., Figure 1; Hubbard et al. 2013). We use the term *degraded* to refer to polygons with high centers and degrading rims (Gamon et al. 2012; Hubbard et al. 2013; Jorgenson and Osterkamp 2005; Liljedahl et al. 2016). Degradation occurs on a continuum, wherein low-centered polygons can start to develop signs of degradation of the rims (e.g., Liljedahl et al. 2016). In this study, area A is characterized by degraded low-centered polygons, area B is degraded high-centered polygons, area C is mixed with a variety of polygon types, area D is undegraded low-centered polygons (e.g., Hubbard et al. 2013; Raz-Yaseef et al. 2017), and the disturbed area is characterized by multiple anthropogenic impacts, in addition to thermal degradation (Gamon et al. 2012). The disturbed area is adjacent to a road that has altered the natural drainage and is characterized by elevated dry areas with dense shrub cover (*Salix pulchra*) intermixed with saturated areas. We refer to the polygons as low-centered undegraded, low-centered degraded, mixed, high-centered degraded, and disturbed.

Measurements

Evapotranspiration was measured with two chambers. One chamber was interfaced with a LI-6400 and the other with a LI-840 Infrared Gas Analyzer (IRGA; this two-chamber approach is similar to Cable et al. [2008]); both IRGAs measure CO_2 and H_2O vapor (LiCor, Lincoln, NE). Both chambers were constructed from clear plexiglas. A cylindrical chamber was attached to the bottom of the LI-6400 soil respiration chamber (total chamber volume of 1.69 L, ground surface area of 0.0085 m^2, after Raz-Yaseef, Rotenberg, and Yakir [2010]). This modified chamber system was utilized with the LI-6400 console the same way the soil respiration system is used for soil CO_2 flux measurements. The second chamber was cube shaped (total chamber volume of 11.42 L, ground surface area of 0.056 m^2) and interfaced with the LI-840 analyzer (LiCor, Lincoln, NE) in a closed-loop configuration with a flow meter (operated at 0.5 L min^{-1}) and a small pump. The chambers were calibrated to each other in the lab using moss that was at field saturation; thirteen paired measurements were made during a period of approximately 60 min. Two calibrations were carried out in the lab. (1) Both chambers were compared with a balance approach to determine if a correction was required. Water was added to sand, measured with each chamber, and then weighed throughout the course of several hours. The LI-840 system did not require a calibration or correction factor relative to the balance, but the LI-6400 data required a correction of 1.6969 applied to the fluxes. We are unsure of why the two chambers differed in requiring a correction. (2) After the correction factor from the balance calibration was applied, the LI-6400 field data were standardized to the LI-840 data, similar to Cable et al. (2008). We used the ratio between the paired measurements to determine a correction factor of 0.6304 and thereafter applied this factor to the LI-6400 data to standardize its measurements to the LI-840 data (wherein, [standardized 6400 data] = 0.6304 × [observed 6400 data]).

Two week-long field campaigns were conducted in the summers of 2013 (late July, days 205–208) and 2014 (early July, days 189–193), and daily measurements were conducted from approximately 9:00 to 17:00 AKST in nonraining conditions (solar noon approximately 14:30). In 2013, measurements focused on capturing variability in water flux across the different polygon types. In 2014, measurements focused on capturing variability in ET associated with the microtopography of the polygons—center, rim, and trough. Both vascular and nonvascular plants were measured, including sedges, grasses, shrubs, mosses, and lichens. Leaf area index (LAI) and biomass were quantified for all the vascular species within the chamber measurement areas for each plot through destructive harvest. Biomass was determined for the nonvascular species.

For ET measurements, the chambers were placed on the ground (LI-840 system) or on a soil collar (LI-6400 system) for 30–60 sec. The flux density (mmol H_2O m^{-2} s^{-1}) was calculated from the slope of H_2O versus time based on Pearcy et al. (1990). Both chambers were used in 2013 but only the LI-840 chamber was used in 2014. Leaf-level conductance (SC-1 porometer, Decagon Devices, Pullman, WA) was measured on the dominant vascular plant species located within the chamber measurement area. Transpiration (mmol H_2O m^{-2} s^{-1}) was calculated from the stomatal conductance measurements (LiCor 1600 porometer manual, LiCor, Lincoln, NE). We made concomitant measurements of soil moisture (0–12 cm depth, both gravimetrically and with a Hydrosense, HSII, Campbell Scientific, Logan, UT, calibrated to soil from the field), soil temperature (Omega Engineering, ON-403-PP,

5–10 cm depth), and surface temperature using a thermal infrared camera (FLIR T620, FLIR Systems, Wilsonville, OR). The thermal infrared imagery was taken for the area encompassed by the chambers. The soil moisture data were rescaled to fractions relative to saturation (saturated soil moisture = 1.0) after Liljedahl et al. (2011), making moisture contents from highly heterogeneous soil types more comparable (Laio et al. 2001). Wind speed and direction, air temperature and relative humidity, pressure, and radiation were measured at an eddy covariance tower located within the measurement area (see Billesbach et al. [2004] for details).

Transpiration measurements were scaled to the chamber area for each plot by multiplying the transpiration data for each species by the associated LAI value, and then summing across all the species measured within the chamber area (for a given plot). Evaporation rates were determined from subtracting transpiration from ET for each observation (evaporation = ET – transpiration). The ET data chamber data were partitioned into transpiration (T) and evaporation (E) components (f_T = (T/ET) × 100, f_E = 100 − f_T, where f is the fraction of ET attributed to T [f_T] or E [f_E]). Ground that was entirely moss or lichen covered (and E dominated) was assigned a T of 0 (f_E value of 1).

Evapotranspiration has diurnal variability, wherein the fluxes peak in the midday and are low in the morning and evening (as observed at the BEO eddy covariance station; Raz-Yaseef et al. 2017). To account for the effect of the time of day that the measurements were conducted, we standardized each chamber ET and transpiration measurement to the eddy covariance station. The maximum daily ET fluxes occurred at approximately 16:00 AKST each day during the week of field measurements (9:00–15:00) each year. We determined the diurnal trend from the tower ET flux data as the difference in ET (in %) between each half-hour measurement and 16:00. Then, utilizing the time stamp associated with each of our chamber flux measurements, our chamber ET measurements were standardized to 16:00 based on the percent determined from the tower. A review of the eddy covariance ET data can be found in Raz-Yaseef et al. (2017).

Data analysis

Despite the measurement plots differing in plant functional types, preliminary data analysis revealed that there was little to no variability between the different plant functional types (2013) and polygon positions (2014). This provided the opportunity to compare the data

between the sampling periods of 2013 and 2014 by polygon type. We utilized a Bayesian statistical analysis approach to account for data and model uncertainty within the ET flux and partitioning regression analyses. With this framework, we conducted regression analyses on the ET data and f_T (partitioning data) from 2013 and 2014. We explored covariance with soil and surface temperature, soil moisture (relative to saturation), and vapor pressure deficit (VPD) in the analyses, and found that soil moisture and surface temperature provided the best fit between observed and predicted ET and f_T. For the ET model, all the measurements for ET and f_T (i = 299) were used. For the f_T analysis, the purely evaporative sites (moss and lichen) were excluded (i = 215).

$$\begin{bmatrix} ET_i \\ f_{T[i]} \end{bmatrix} \sim \begin{bmatrix} \mu_{ET[i]}, \tau_{ET} \\ \mu_{f.T[i]}, \tau_{f.T} \end{bmatrix} \tag{1}$$

The mean of each data model in equation 1 is given by μ and the precision by τ. The mean model for each dataset is given a regression equation with some or all of the parameters (a, b, c, and d in equations 2–5) varying by plot (n = 5, *polygon*). Thus, for n observations,

$$\mu_{ET[i]} = a_{1,year} + a_{2,year,polygon} \cdot SM_i + a_{3,year,polygon} \cdot T_i \tag{2}$$

$$\mu_{f.T[i]} = b_{1,year,polygon} + b_{2,year} \cdot SM_i + b_{3,year} \cdot T_i \\ + b_{4,year} \cdot (T_i \cdot SM_i) \tag{3}$$

In each regression, the soil moisture (SM) and soil temperature (T) data are mean centered, wherein the mean is subtracted from each observation of SM and T, respectively. This aids in estimating and interpreting the intercept terms (a_1, b_1). In the regressions for both ET and f_T (equations 2 and 3), the effects of both SM and T on ET are quantified. In the regression for f_T (equation 3), the interactive effects of SM and T on ET are also quantified. In the regression for ET (equation 2), the intercept varies by year, and the effects of SM and T (a_2 and a_3) vary by polygon and year. In the regression for f_T (equation 3), the intercept varies by year and polygon, and the effects of soil moisture and temperature (b_2, b_3, b_4) vary by year.

Finally, we conducted ANOVAs on the field data (ET, transpiration, f_T, soil moisture relative to saturation, and soil temperature) to compare differences across polygons, years, and microtopographic positions. The ANOVAs were also conducted in a Bayesian framework. All parameters were given independent noninformative priors with a normal distribution, and were centered on a mean of 0 and a precision of 0.0001 ([a, b, c, d, e] ~ Normal [0, 0.0001]). The precisions were calculated from the standard deviations ($\tau = \sigma^{-2}$) and the σs were given uniform priors with a wide range (σ ~ Uniform [0, 10]). The models were run in OpenBUGS

with four chains yielding more than 5,000 samples for quantifying posterior statistics.

Results

Temperature and moisture

The data from the eddy covariance tower show that the summer (June–August) air temperature in 2013 was higher compared to 2014 (mean [standard error]; 4.1° C [0.07] vs. 1.7 °C [0.05]); likewise, the soil temperature near the eddy covariance tower was higher in 2013 relative to 2014 (5.7 [0.08] vs. 2.9 [0.06], respectively). The VPD was similar between years (2013: 4.21 kPa [0.06]; 2014: 4.23 kPa [0.05]). Plot-level soil moisture was higher in the 2014 sampling period compared to 2013 in all but the mixed and disturbed polygons, with the highest soil moisture occurring in the low-centered undegraded polygons (Figure 2A, Tables 1 and 2). Soils were saturated in the troughs across all polygon types (2014, Figure 2B). Comparing the centers and rims across polygons, soil moisture was highest in the low-
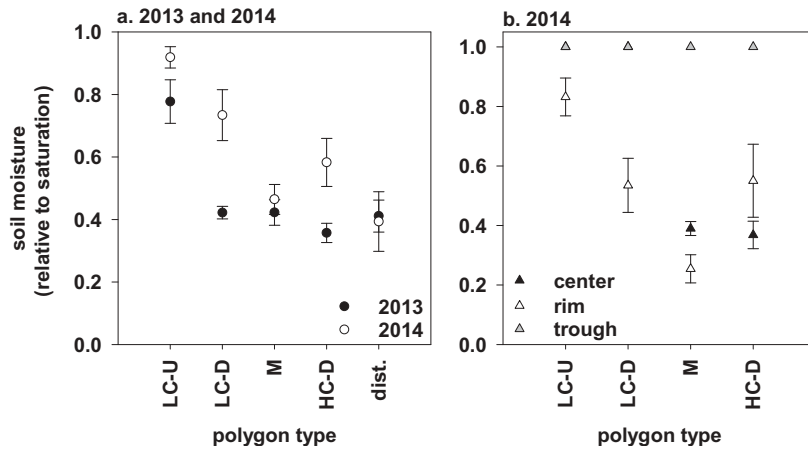

Figure 2. Means and standard errors are shown for (A) soil moisture relative to saturation for measurement days 205–207 (2013) and 189–193 (2014) across the polygon types, and (B) soil moisture from 2014 across the different positions within each polygon type. Soil moisture data (cm^3/cm^3) are relative to saturation for the soil type within which the field measurement was taken. Soil moisture values near 1.0 indicate that the soils are saturated, and values near 0.5 indicate that soils are at 50 percent saturation, and so on. The different polygon types are: low-centered undegraded (LC-U), low-centered degraded (LC-D), mix of high- and low-center polygons (M), high-centered degraded (HC-D), and disturbed. The different positions indicated are: the center of a polygon (center), the rim of a polygon (rim), and the troughs between polygons (trough).

Table 1. Mean and 95 percent credible intervals for each data set for measurement days 205–207 (2013) and 189–193 (2014). Results from the ANOVAs are shown, wherein differences between years are denoted with a superscript A or B. ET is evapotranspiration, T/ET is the fraction of ET that is transpiration, VPD is vapor pressure deficit.

Data		Measurement Year (Mean and 95% CI)	
		2013	2014
ET	mmol m^{-2} s^{-1}	0.07 [0.06, 0.08][A]	0.02 [0.005, 0.03][B]
ET	*mm hr^{-1}	0.0045 [0.0039, 0.0051]	0.0013 [0.0003, 0.0019]
ET	*mm day^{-1}	0.11 [0.09, 0.12]	0.03 [0.008, 0.047]
Transpiration	mmol m^{-2} s^{-1}	0.008 [0.006, 0.009][A]	4×10^{-5} [0, 0.002][B]
Transpiration	*mm hr^{-1}	0.0005 [0.0004, 0.0006]	2.6×10^{-6} [0, 0.0001]
Transpiration	*mm day^{-1}	0.012 [0.009, 0.014]	6.2×10^{-6} [0, 0.003]
Evaporation	mmol m^{-2} s^{-1}	0.07 [0.06, 0.08][A]	0.02 [0.005, 0.03][B]
Evaporation	*mm hr^{-1}	0.0045 [0.0039, 0.0051]	0.0013 [0.0003, 0.0019]
Evaporation	*mm day^{-1}	0.11 [0.09, 0.12]	0.03 [0.008, 0.047]
T/ET		0.23 [0.18, 0.27][A]	0.03 [0, 0.09][B]
Soil moisture (relative to saturation)		0.46 [0.41, 0.50][B]	0.62 [0.56, 0.67][A]
VPD (kPa)		0.030 [0.026, 0.033][B]	0.034 [0.030, 0.039][A]
Soil temperature (°C) 5–10 cm		4.08 [3.9, 4.3]	4.04 [3.75, 4.32]
Air temperature (°C)		2.27 [2.11, 2.44][A]	1.72 [1.49, 1.93][B]
Surface temperature (°C)		7.71 [7.17, 8.23][B]	9.43 [8.72, 10.09][A]
Cumulative rainfall (mm)		19.3[A]	0.51[B]

*We did not make diurnal measurements so the daily values should be considered an estimate. The estimate per hour (mm hr−1) should be considered only during the time of day that measurements were taken.

Table 2. Mean and 95 percent credible intervals for each data set for the different polygon features measurement days 205–207 (2013) and 189–193 (2014). Results from the ANOVAs are shown, where the 95 percent credible intervals do not overlap the means of other polygons or years denotes statistically significant differences. ET = evapotranspiration; T/ET = the fraction of ET that is transpiration; soil T and surface T = temperatures. The different polygon types are: low-centered undegraded (LC-U), low-centered degraded (LC-D), mix of high- and low-center polygons (M), high-centered degraded (HC-D), and disturbed. The results for 2014 are averages across the polygon position (center, rim, trough).

| | Polygon Type and Year | | | | | | | | | |
| | LC-U | | LC-D | | M | | HC-D | | Disturbed | |
Data	2013	2014	2013	2014	2013	2014	2013	2014	2013	2014
ET mmol m^{-2} s^{-1}	0.04 [0.01, 0.06]	0.02 [8 × 10^{-4}, 0.04]	0.06 [0.04, 0.08]	0.02 [7 × 10^{-4}, 0.04]	0.07 [0.05, 0.09]	0.02 [0.002, 0.04]	0.10 [0.08, 0.12]	0.02 [8 × 10^{-4}, 0.04]	0.09 [0.07, 0.11]	0.06 [0.02, 0.09]
Transpiration mmol m^{-2} s^{-1}	0.02 [0.02, 0.03]	0.002 [0, 0.004]	0.001 [0, 0.004]	0.002 [0, 0.006]	0.002 [0, 0.005]	0.001 [0, 0.004]	0.002 [0, 0.004]	0.002 [0, 0.006]	0.02 [0.02, 0.03]	0.002 [0, 0.006]
Evaporation mmol m^{-2} s^{-1}	0.02 [0.002, 0.04]	0.02 [0.001, 0.04]	0.06 [0.04, 0.08]	0.02 [6 × 10^{-4}, 0.04]	0.07 [0.05, 0.09]	0.02 [0.002, 0.04]	0.10 [0.08, 0.12]	0.02 [7 × 10^{-4}, 0.04]	0.07 [0.05, 0.10]	0.06 [0.03, 0.09]
T/ET	0.72 [0.63, 0.81]	0.04 [0.002, 0.11]	0.07, [0.01, 0.14]	0.07 [0.004, 0.18]	0.13 [0.05, 0.20]	0.04 [0.002, 0.10]	0.07 [0.01, 0.15]	0.07 [0.004, 0.17]	0.33 [0.25, 0.41]	0.10 [0.008, 0.22]
Soil moisture (relative to saturation)	0.78 [0.67, 0.88]	0.92 [0.82, 1.00]	0.42 [0.34, 0.50]	0.73, [0.59, 0.88]	0.42 [0.34, 0.50]	0.46 [0.38, 0.55]	0.36 [0.27, 0.44]	0.58 [0.45, 0.72]	0.41 [0.32, 0.50]	0.40 [0.26, 0.53]
Soil T (°C) 5–10 cm	3.12 [2.70, 3.53]	3.77 [3.04, 4.51]	3.96 [3.54, 4.38]	2.74 [2.03, 3.39]	4.4 [3.98, 4.83]	3.41 [2.99, 3.83]	4.22 [3.71, 4.73]	4.94 [4.41, 5.45]	4.82 [4.38, 5.27]	5.68 [5.00, 6.39]
Surface T (°C)	6.80 [5.87, 7.72]	7.62 [6.06, 9.22]	10.0 [9.09, 10.9]	6.94 [5.48, 8.44]	6.34 [5.43, 7.25]	8.12 [7.14, 9.06]	6.76 [5.65, 7.87]	9.39 [8.23, 10.5]	8.32 [7.37, 9.32]	17.3 [15.77, 18.87]

centered undegraded and lowest in the mixed (Figure 2B).

Soil temperatures were highest in the disturbed polygons, particularly in the 2014 sampling period (Figure 3A, Table 2). The lowest soil temperatures in each year occurred in the low-centered degraded (2013) and high-centered degraded (2014) polygons (Figure 3A, Table 2). In 2014, the highest soil temperatures occurred in the troughs (compared to the rims and centers; Figure 3C). The largest variation in temperatures occurred in the low-centered degraded polygons (3°C difference across the center, rim, and troughs; Figure 3C), and the low-centered undegraded showed the least variation (1°C difference, Figure 3B). Surface temperatures ranged from 7.5–10°C for all but the disturbed polygon (17°C in the 2013 sampling period, Figure 3B, Table 2). There was little variation in surface temperatures across the edges, centers, and troughs (Figure 3D).

Leaf area index (LAI)

The leaf area and biomass data are shown in Table 3. Leaf area index ranged from less than 0.2 to 2.55 m²/m², with the highest LAI occurring in the disturbed polygons (*Arctophila fulva* and *S. pulchra*). For non-vascular plants, moss had more biomass in the plots than lichen. Lichen biomass was greatest in the low- and high-centered degraded polygons and it was least in the undegraded polygons. Moss biomass was high in all but the low-centered degraded polygon.

Evapotranspiration, transpiration, evaporation

Evapotranspiration rates were four times higher during the sampling period in 2013 compared to the 2014 sampling period (Figure 4A, Table1). On average across both sampling periods and all polygons, evaporation composed more than 90 percent of the ET flux
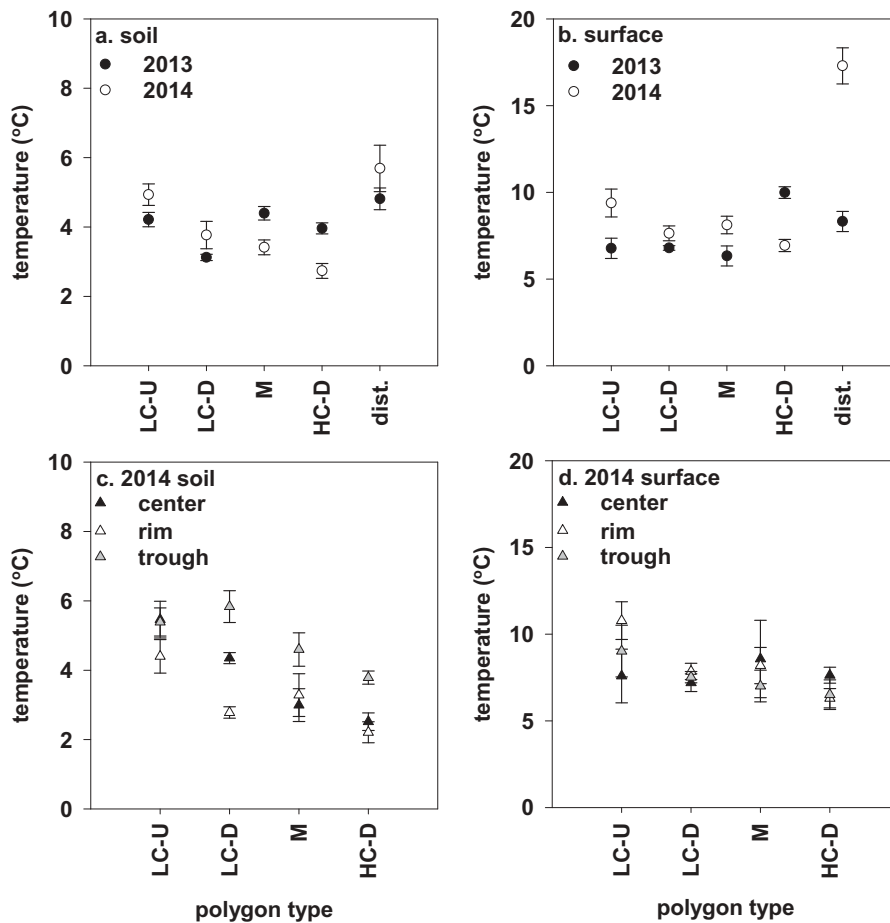
Figure 3. Means and standard errors are shown for soil temperature (°C) data from 5–10 cm depth (panels A, C) and surface temperature (°C) data collected with thermal infrared measurements (B, D). Panels A and B show data collected during measurement days 205–207 (2013) and 189–193 (2014) for the different polygon types progressing from least degraded to the disturbed (*dist*) polygons. Panels C and D are data from the different positions—center, rim, and trough—for each polygon in 2014. The different polygon types are: low-centered undegraded (LC-U), low-centered degraded (LC-D), mix of high- and low-center polygons (M), high-centered degraded (HC-D), and disturbed.

Table 3. Means and standard errors of leaf area index (LAI, m^2/m^2) and biomass (g/m^2) values for vascular and non-vascular plants found in the different polygons and polygon positions (data were collected in late July 2014 only). The different polygon types are low-centered undegraded (LC-U), low-centered degraded (LC-D), mix of high- and low-center polygons (M), high-centered degraded (HC-D), and disturbed.

Species LAI (m^2/m^2)	Polygon				
	LC-U	LC-D	M	HC-D	Disturbed
A. latifolia	NA	NA	NA	NA	0.36 [0.08]
A. fulva	NA	NA	NA	NA	2.42 [0.88]
C. aquatilis 2013	1.24 [0.49]	0.63 [0.08]	0.26 [0.08]	0.19 [0]	0.31 [0.14]
C. aquatilis 2014 Center	0.014 [0.001]	0.006 [0.0008]	0.006 [0.0004]	0.005 [0.0008]	NA
C. aquatilis 2014 Edge	0.003 [0.0007]	0.005 [0.0006]	0.011 [0.0005]	0.004 [0.0008]	NA
C. aquatilis 2014 Trough	0.011 [0.002]	0.006 [0.0009]	0.012 [0.0006]	0.012 [0.002]	NA
E. angustifolium 2013	NA	NA	0.89 [0.42]	NA	1.12 [0.62]
E. angustifolium 2014	NA	NA	NA	0.0008 [0] center only	0.02 [0.002]
E. russeolum	NA	0.64 [0.18]	0.027 [0]	NA	NA
L. arctica	NA	0.32 [0.12]	0.060 [0.02]	0.12 [0.10]	0.052 [0.03]
P. frigidus	0.044 [0.01]	NA	NA	0.657 [0.02]	NA
P. arctica	0.022 [0.01]	0.026 [0]	0.16 [0.07]	0.0121 [0]	0.076 [0.06]
S. pulchra 2013	NA	NA	1.06 [0.33]	NA	2.75 [1.03]
S. pulchra 2014					0.025 [0.002]
S. pulchra 2014 Center	NA	NA	0.013 [0.002]	NA	NA
S. pulchra 2014 Edge	NA	NA	0.014 [0.010]	NA	NA
S. rotundifolia	0.51 [0.20]	NA	NA	NA	NA
V. vitis-idaea	NA	NA	NA	0.559 [0.14]	NA
Biomass (g/m^2)					
Moss	187.9 [90.5]	131.5 [29.6]	192.0 [73.3]	208.9 [42.5]	235.8 [90.5]
Lichen	1.02 [0]	108.6 [31.9]	32.96 [13.5]	101.5 [18.3]	61.6 [18.9]

(Figure 4F, Table 2). Although transpiration rates were much higher in 2013 compared to 2014, evaporation rates drove the differences in ET between sampling periods (Figures 4A, B). Transpiration was 20 percent of the ET flux in 2013 but was less than 5 percent in 2014 (Figure 4B, Table 1). In 2013, ET rates were largest in the high-centered degraded and disturbed polygons and lowest in the low-centered undegraded polygons (Figure 4C, Table 2). Transpiration rates were largest in the disturbed and low-centered undegraded polygons (Figure 4C, Table 2). Evaporation dominated the ET flux in all but the low-centered undegraded polygons, where transpiration composed approximately 70 percent of the ET flux (Figure 4D, Table 2). In the disturbed polygons, transpiration composed 30 percent of the ET flux but less than 10 percent of ET in the remaining polygons (Figure 4D, Table 2). In 2014, ET was highest in the disturbed polygons and lowest the low- and high-centered degraded polygons (Figure 4E, Table 2).

Comparisons across polygon microtopography (only in the 2014 sampling period) reveal that ET is highest in the centers of low-centered undegraded polygons and lowest in the low-centered degraded polygons (Figure 5B). In all the polygon centers, evaporation dominated the ET flux (>95%, Figure 5B). Comparisons of the polygon rims reveal that ET was highest in the mixed polygons and lowest in the low- and high-centered degraded polygons (Figure 5C). Across all the rims and troughs, evaporation dominated the ET flux (>95%, Figures 5D, E). Even though evaporation dominated the ET fluxes across the troughs, transpiration composed a greater proportion of ET (~18%) in the troughs of high-centered degraded polygons compared to the troughs of the other polygons (<5%, Figure 5F).

Regression analyses

The parameters in the ET regression analysis explained approximately 44 percent of the variability in the data ($R^2 = 0.44$) and the parameter estimates are found in Table 4. Across all the polygons, ET under average surface temperature and moisture conditions (the intercept) was three times greater in the 2013 sampling period compared to 2014. Surface temperature impacted ET more in 2013 compared to 2014. Warmer soils increased ET in the disturbed polygons to a greater extent than the high-centered degraded and
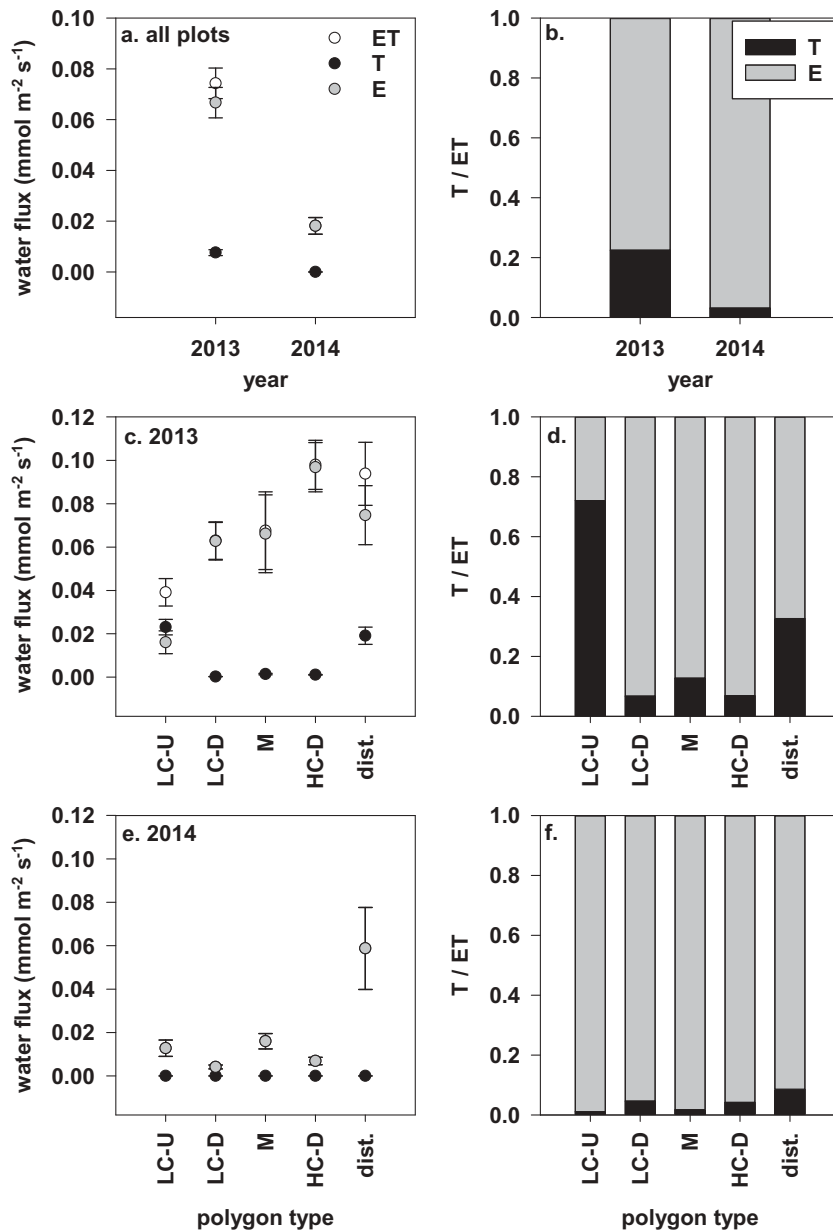
Figure 4. Means and standard errors for the evapotranspiration (ET) rates and means for the partitioning into evaporation (E) and transpiration (T) for both years (A, B), 2013 (C, D), and 2014 (E, F) across the polygon degradation gradient (D = least degraded, disturbed = most degraded). Data are from measurement days 205–207 (2013) and 189–193 (2014). The different polygon types are: low-centered undegraded (LC-U), low-centered degraded (LC-D), mix of high- and low-center polygons (M), high-centered degraded (HC-D), and disturbed.

mixed polygons. In 2014, warmer soils increased ET only in the disturbed polygons. Similar to surface temperature, soil moisture impacted ET more in 2013 compared to 2014. In 2013, higher soil moisture increased ET in the mixed and disturbed polygons but decreased ET in the high-centered degraded polygons. Unlike the temperature effects, soil moisture impacted ET in the mixed polygons to a greater extent than the high-centered degraded and disturbed polygons. In

2014, high soil moisture increased ET only in the disturbed polygons.

The parameters in the ET partitioning regression analysis explained 55 percent of the variability in the data ($R^2 = 0.55$), and the parameter estimates are found in Table 5. The contribution of transpiration to ET under average soil moisture and surface temperature conditions (the intercept) was similar across polygons in the 2014 sampling period. In the 2013 sampling period, the
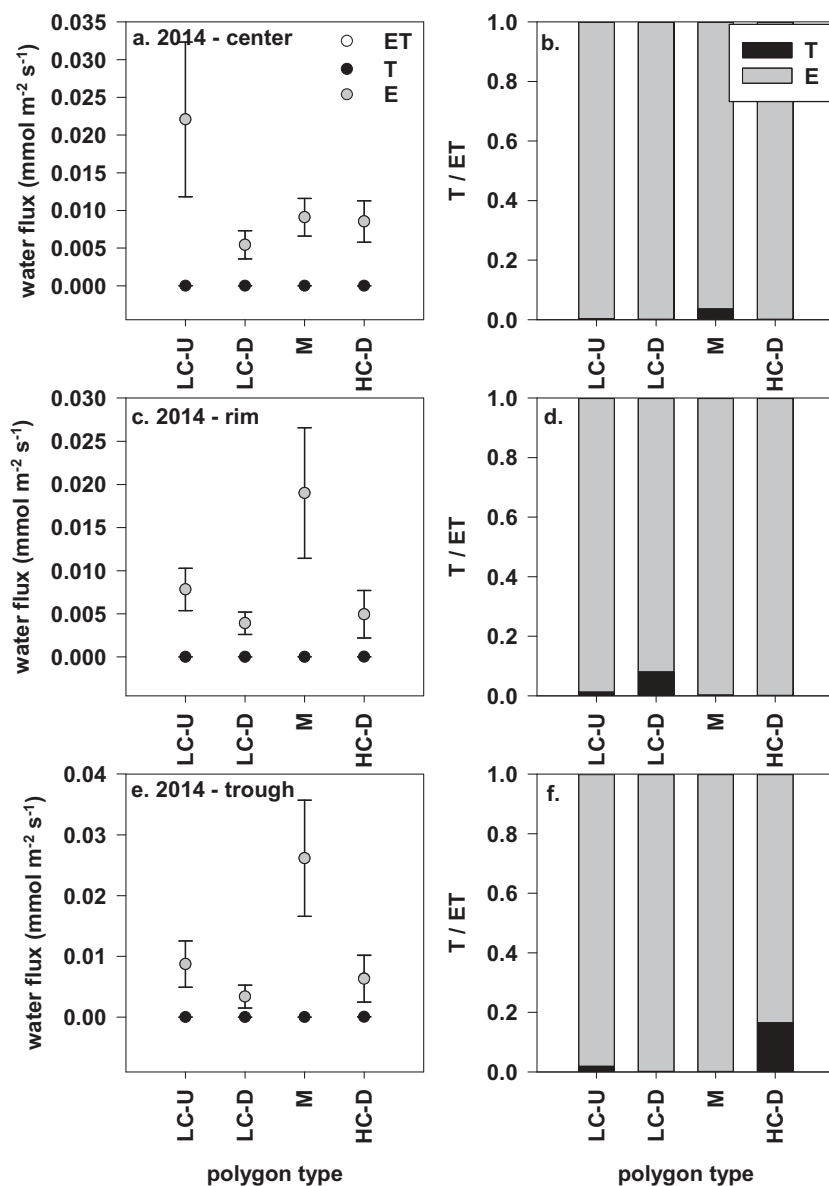
Figure 5. Means and standard errors for the water flux rates and means for the evapotranspiration (ET) partitioning into evaporation (E) and transpiration (T) for 2014 in the different polygon features (polygon center in panels A and B, polygon edge in panels C and D, and polygon trough in panels E and F) across the polygon degradation gradient (D = least degraded, disturbed = most degraded). Data are from measurement days 205–207 (2013) and 189–193 (2014). The different polygon types are: low-centered undegraded (LC-U), low-centered degraded (LC-D), mix of high- and low-center polygons (M), high-centered degraded (HC-D), and disturbed.

highest contributions of transpiration to ET occurred in the low-centered undegraded polygons, followed by the disturbed, high-centered degraded, mixed, and low-centered degraded polygons. Soil moisture and surface temperatures did not explain the variability in the partitioning data in 2014, likely because of low transpiration rates. In 2013, soil moisture and surface temperature impacted the contribution of transpiration to ET. First, the singular effects showed that higher soil moisture increased the contribution of transpiration to ET, but higher surface temperature increased the contribution of evaporation to ET. Second, with a positive interaction effect, higher soil moisture combined with higher surface temperature increased the contribution of transpiration to ET.

Discussion

The goal of this study was to assess the ET dynamics, including the partitioning of evaporation and transpiration, of different microtopographies created by polygonal ground across a gradient in permafrost geomorphology. We found that ET was higher in the

Table 4. The estimated means and 95 percent credible intervals for the parameters in the evapotranspiration (ET) regression model. The intercept (a_1) only varied by year, but a_2 (surface temperature effect) and a_3 (soil moisture effect) varied by year and polygon type. Statistical differences between polygon types are denoted by capital letters, and parameter values that are statistically different from zero are in bold. The italicized values are those that are marginally significant, as the 95 percent credible interval narrowly overlaps zero. The different polygon types are low-centered undegraded (LC-U), low-centered degraded (LC-D), mix of high- and low-center polygons (M), high-centered degraded (HC-D), and disturbed.

Year	a_1 (Intercept)	Polygon Type	a_2 (Surface Temperature Effect)	a_3 (Soil Moisture Effect)
2013	0.06 [0.04, 0.07][A]	LC-U	−0.002 [−0.008, 0.005]	−0.02 [−0.08, 0.03]
		LC-D	0.0007 [−0.009, 0.011]	−0.09 [−0.23, 0.05]
		M	**0.008 [0.004, 0.013][B]**	**0.17 [0.10, 0.24][A]**
		HC-D	*0.003 [−0.0008, 0.007][C]*	**−0.14 [−0.22, −0.06][C]**
		Disturbed	**0.016 [0.011, 0.020][A]**	**0.09 [0.02, 0.15][B]**
2014	0.02 [0.001, 0.04][B]	LC-U	0.0005 [−0.004, 0.005]	−0.01 [−0.08, 0.06]
		LC-D	−0.003 [−0.013, 0.007]	−0.01 [−0.10, 0.08]
		M	0.0005 [−0.005, 0.005]	0.003 [−0.06, 0.07]
		HC-D	−0.003 [−0.015, 0.009]	−0.01 [−0.10, 0.08]
		Disturbed	0.005 [0.002, 0.007]	0.20 [0.11, 0.28]

Table 5. Means and 95 percent credible intervals for the parameters in the evapotranspiration (ET) partitioning regression model. The intercept (a_1) varied by year and polygon type, but a_2 (soil moisture effect), a_3 (surface temperature effect), and a_4 (interaction effect) varied by year. Statistical differences between polygon types are denoted by capital letters, and parameter values that are statistically different from zero are in bold. The different polygon types are low-centered undegraded (LC-U), low-centered degraded (LC-D), mix of high- and low-center polygons (M), high-centered degraded (HC-D), and disturbed.

Year	Polygon Type	a_1 (Intercept)	a_2 (Soil Moisture Effect)	a_3 (Surface Temperature Effect)	a_4 (Surface Temperature × Soil Moisture)
2013	LC-U	0.61[0.5, 0.71][A]	**0.34 [0.18, 0.50]**	**−0.03 [−0.04, −0.009]**	**0.06 [0.02, 0.11]**
	LC-D	0.05 [0.002, 0.15][D]			
	M	0.08 [0.009, 0.17][CD]			
	HC-D	0.16 [0.06, 0.25][C]			
	Disturbed	0.48 [0.38, 0.57][B]			
2014	LC-U	0.07 [0.003, 0.18]	−0.07 [−0.24, 0.10]	0.002 [−0.01, 0.02]	−0.02 [−0.06, 0.02]
	LC-D	0.10 [0.007, 0.25]			
	M	0.04 [0.002, 0.11]			
	HC-D	0.09 [0.005, 0.21]			
	Disturbed	0.14 [0.008, 0.33]			

2013 sampling period compared to 2014, evaporation generally dominated the ET flux, and ET was greatest in the drier polygons (contrary to our hypothesis). Evapotranspiration rates observed in this study range from approximately 0.06 mm hour^{-1} (minimum 09:00–10:00) to approximately 6.5 mm hour^{-1} (maximum 15:00–16:00), which is on par with prior work on the Arctic Coastal Plain (Dery et al. 2005; Mendez, Hinzman, and Kane 1998). However, the ET rates observed on the Arctic Coastal Plain during the field sampling periods (0.001–0.10 mmol m^{-2} s^{-1}) are much lower compared to other northern latitude systems (Siberian forest and bog, 1.1–2.5 mmol m^{-2} s^{-1}; Valentini et al. 2000).

Evapotranspiration and transpiration rates greatly differed between the two sampling periods (years), with the drier and warmer sampling period (2013) having much higher rates than the wetter and colder sampling period (2014, Figure 4). This is in contrast to

Vourlitis and Oechel (1997), who found minimal year-to-year variability in ET fluxes measured during two summers. We found that warmer surface temperatures were associated with higher ET rates in the more degraded polygons (mixed, high-centered degraded, and disturbed; Table 4), which is not surprising because any increase in temperature in a cold environment should increase water fluxes. The observed positive relationship between soil moisture and ET is expected for the drier polygons (disturbed and mixed), but the negative relationship with ET observed in the equally dry high-centered degraded polygon is unexpected (Table 4). This negative moisture relationship may be because of the complex relationship between ET fluxes, soil moisture, and soil temperature. Energy available for ET may be reduced because ground heat flux in cold, wet soils is the predominant energy sink (Liljedahl et al. 2011). Thus, while the high-centered degraded polygons are drier compared to the other polygons, they

are still relatively cold and wet (e.g., Table 2). Our primary findings—that ET is higher with wetter and warmer soils in the degrading areas—suggest that there may be a threshold of soil moisture with higher temperatures, wherein as the polygon soils shift from wetter to drier (and warmer) with permafrost thaw, ET may tend to increase.

Evapotranspiration partitioning into evaporation and transpiration provides more information about the primary controls on ET, and is a key advantage of combining chamber and leaf-level measurements. Evaporation dominated the ET flux, a trend that was greater in the colder and wetter sampling period (2014, >90%) compared to the warmer and drier one (2013, 80%; Figures 4A, B, Table 1). In the warmer and drier sampling period, transpiration contributed more to ET under warmer and wetter soil conditions (Table 5). Warmer soil temperatures stimulate stomatal conductance and transpiration in arctic tundra vegetation (Tenhunen et al. 1992). Tundra plants reach peak stomatal conductance at about air temperatures of 10–20° C, but many species can function down to 0°C (Oberbauer and Dawson 1992; Tenhunen et al. 1992). With the approximately 2°C air temperatures during the study period (Table 1), the plants may have been functioning at suboptimal levels. However, the conductance rates in this study were on par with those measured by others (0.02–0.35 mol m^{-2} s^{-1} in this study, 0.05–0.4 mol m^{-2} s^{-1}, summarized by Oberbauer and Dawson 1992). The observed temperature effect on ET partitioning does not necessarily relate to permafrost degradation, because the low-centered undegraded polygons had the highest partitioning to transpiration (~75%, 2013), followed by the disturbed and mixed polygons (~10–35%, Figure 4). However, our findings suggest that higher soil temperatures associated with permafrost thaw may result in a greater fraction of ET flux attributed to transpiration. Increased transpiration can reduce subsurface soil moisture and alter the timing of the response of ET to precipitation (e.g., Kane et al. 1992; Lawrence et al. 2007). Increased transpiration can also impact how ET is represented in large-scale climate models (e.g., Lawrence et al. 2007).

While we did not explicitly explore the impact of different plant functional types on ET rates and partitioning, it is worth noting that there is high deciduous shrub (S. pulchra) LAI in the disturbed polygons (Table 3). The LAI associated with these plots is 60 percent higher than the peak LAI reported by others (Wielgolaski et al. 1981). Shrubby ground had high ET rates and partitioning of ET to transpiration (30% in

2013, 10% in 2014). Clearly there is more work to be done on this topic, including examining seasonal trends in LAI, ET, and partitioning to transpiration across years with contrasting weather conditions. However, anecdotally our work suggests that as deciduous shrubs continue to encroach on the Arctic tundra (Sturm, Racine, and Tape 2001; Tape, Sturm, and Racine 2006), ET flux and the fraction of ET attributed to transpiration may increase.

Microtopography associated with the center, trough, and rims of polygons is likely an important factor affecting ET fluxes, as others have found that microtopography in tundra landscapes can affect plant diversity, soil moisture, and CO_2 fluxes (Engstrom et al. 2006; Gamon et al. 2013; Lee, Schuur, and Vogel 2010). However, limited variability in the 2014 data did not allow us to quantify the response of ET fluxes of polygon centers, troughs, and rims to soil moisture and temperature, and this limits our confidence in drawing definitive conclusions (e.g., Figure 5).

In summary, we found that during peak leaf area (July) of two contrasting years, evaporation dominated the ET flux. Given the significant differences in ET rates between sampling periods (years), we suspect that if the soils of the Alaskan Arctic Coastal Plain warm and dry with changes in permafrost, ET will tend to increase to a certain point. Yet, after a threshold is reached, additional moisture and higher temperatures will be required to further stimulate ET. While it is unlikely that transpiration will completely dominate the ET flux in the near future, warmer soil temperatures and greater shrub cover may increase the contribution of transpiration to ET compared to the present. This shift may change the way ET is modeled at the landscape scale.

Acknowledgments

Funding

References

Betts, A. K., M. Goulden, and S. Wofsy. 1999. Controls on evaporation in a boreal spruce forest. *Journal of Climate* 12 (6):1601–18.

Billesbach, D., M. Fischer, M. Torn, and J. Berry. 2004. A portable eddy covariance system for the measurement of ecosystem: Atmosphere exchange of CO_2, water vapor, and energy. *Journal of Atmospheric and Oceanic Technology* 21 (4):639–50.

Cable, J. M., K. Ogle, D. G. Williams, J. F. Weltzin, and T. E. Huxman. 2008. Soil texture drives responses of soil respiration to precipitation pulses in the Sonoran Desert: Implications for climate change. *Ecosystems* 11 (6):961–79.

Calder, I. R. 1998. Water use by forests, limits and controls. *Tree Physiology* 18 (8–9):625–31.

Dery, S. J., M. Stieglitz, A. K. Rennermalm, and E. F. Wood. 2005. The water budget of the Kuparuk River basin, Alaska. *Journal of Hydrometeorology* 6 (5):633–55.

Engstrom, R., A. Hope, H. Kwon, Y. Harazono, M. Mano, and W. Oechel. 2006. Modeling evapotranspiration in Arctic coastal plain ecosystems using a modified BIOME-BGC model. *Journal of Geophysical Research-Biogeosciences* 111 (G2). doi:10.1029/2005JG000102.

Engstrom, R., A. Hope, H. Kwon, D. Stow, and D. Zamolodchikov. 2005. Spatial distribution of near surface soil moisture and its relationship to microtopography in the Alaskan Arctic coastal plain. *Nordic Hydrology* 36 (3):219–34.

Gamon, J. A., K. F. Huemmrich, R. S. Stone, and C. E. Tweedie. 2013. Spatial and temporal variation in primary productivity (NDVI) of coastal Alaskan tundra: Decreased vegetation growth following earlier snowmelt. *Remote Sensing of Environment* 129:144–53.

Gamon, J. A., G. P. Kershaw, S. Williamson, and D. S. Hik. 2012. Microtopographic patterns in an arctic baydjarakh field: Do fine-grain patterns enforce landscape stability? *Environmental Research Letters* 7 (1):1–6.

Hinzman, L. D., C. J. Deal, A. D. McGuire, S. H. Mernild, I. V. Polyakov, and J. E. Walsh. 2013. Trajectory of the Arctic as an integrated system. *Ecological Applications* 23 (8):1837–68.

Hubbard, S. S., C. Gangodagamage, B. Dafflon, H. Wainwright, J. Peterson, A. Gusmeroli, C. Ulrich, Y. Wu, C. Wilson, and J. Rowland. 2013. Quantifying and relating land-surface and subsurface variability in permafrost environments using LiDAR and surface geophysical datasets. *Hydrogeology Journal* 21 (1):149–69.

Jasechko, S., Z. D. Sharp, J. J. Gibson, S. J. Birks, Y. Yi, and P. J. Fawcett. 2013. Terrestrial water fluxes dominated by transpiration. *Nature* 496 (7445):259–279.

Jorgenson, M. T., and T. E. Osterkamp. 2005. Response of boreal ecosystems to varying modes of permafrost degradation. *Canadian Journal of Forest Research-Revue Canadienne De Recherche Forestiere* 35 (9):2100–11.

Kane, D. L., R. E. Gieck, and L. D. Hinzman. 1990. Evapotranspiration from a small Alaskan Arctic Watershed. *Nordic Hydrology* 21 (4–5):253–72.

Kane, D. L., L. D. Hinzman, R. E. Gieck, J. P. McNamara, E. K. Youcha, and J. A. Oatley. 2008. Contrasting extreme runoff events in areas of continuous permafrost, Arctic Alaska. *Hydrology Research* 39 (4):287–98.

Kane, D. L., L. D. Hinzman, J. P. McNamara, Z. Zhang, and C. S. Benson. 2000. An overview of a nested watershed study in Arctic Alaska. *Nordic Hydrology* 31 (4–5):245–66.

Kane, D. L., L. D. Hinzman, M. Woo, and K. R. Everett. 1992. Arctic hydrology and climate change. In *Arctic ecosystems in a changing climate*, ed. F. S. Chapin, R. L. Jefferies, J. F. Reynolds, G. R. Shaver, and J. Svoboda, 35–55. San Diego, CA: Academic Press.

Kanevskiy, M., Y. Shur, M. T. Jorgenson, C. L. Ping, G. J. Michaelson, D. Fortier, E. Stephani, M. Dillon, and V. Tumskoy. 2013. Ground ice in the upper permafrost of the Beaufort Sea coast of Alaska. *Cold Regions Science and Technology* 85:56–70.

Laio, F., A. Porporato, L. Ridolfi, and I. Rodriguez-Iturbe. 2001. Plants in water-controlled ecosystems: Active role in hydrologic processes and response to water stress–II. Probabilistic soil moisture dynamics. *Advances in Water Resources* 24 (7):707–23.

Lawrence, D. M., P. E. Thornton, K. W. Oleson, and G. B. Bonan. 2007. The partitioning of evapotranspiration into transpiration, soil evaporation, and canopy evaporation in a GCM: Impacts on land-atmosphere interaction. *Journal of Hydrometeorology* 8 (4):862–80.

Lee, H., E. A. G. Schuur, and J. G. Vogel. 2010. Soil CO_2 production in upland tundra where permafrost is thawing. *Journal of Geophysical Research-Biogeosciences* 115 (G1),:1-11.

Liljedahl, A., L. Hinzman, Y. Harazono, D. Zona, C. Tweedie, R. D. Hollister, R. Engstrom, and W. Oechel. 2011. Nonlinear controls on evapotranspiration in arctic coastal wetlands. *Biogeosciences* 8 (11):3375–89.

Liljedahl, A., L. Hinzman, and J. Schulla. 2012. Ice-wedge polygon type controls low-gradient watershed-scale hydrology. In *Proceedings of the Tenth International Conference on Permafrost*, ed. K. M. Hinkel, 231–36. Salekhard, Russia: The Northern Publisher.

Liljedahl, A. K., J. Boike, R. P. Daanen, A. N. Fedorov, G. V. Frost, G. Grosse, L. D. Hinzman, Y. Iijma, J. C. Jorgenson, N. Matveyeva, et al. 2016. Pan-Arctic ice-wedge degradation in warming permafrost and its influence on tundra hydrology. *Nature Geoscience* 9 (4):312–18.

Mendez, J., L. D. Hinzman, and D. L. Kane. 1998. Evapotranspiration from a wetland complex on the Arctic coastal plain of Alaska. *Nordic Hydrology* 29 (4–5):303–30.

Oberbauer, S., and T. E. Dawson. 1992. Water relations of arctic vascular plants. In *Arctic ecosystems in a changing climate: An ecophysiological perspective*, ed. F. S. Chapin, R. L. Jefferies, J. F. Reynolds, G. R. Shaver, and J. Svoboda, 259–79. San Diego, CA: Academic Press.

Oechel, W. C., G. L. Vourlitis, S. Brooks, T. L. Crawford, and E. Dumas. 1998. Intercomparison among chamber, tower, and aircraft net CO_2 and energy fluxes measured during the Arctic System Science Land-Atmosphere-Ice Interactions (ARCSS-LAII) flux study. *Journal of Geophysical Research-Atmospheres* 103 (D22):28993–9003.

Olivas, P. C., S. F. Oberbauer, C. Tweedie, W. C. Oechel, D. Lin, and A. Kuchy. 2011. Effects of fine-scale topography on CO_2 flux components of Alaskan Coastal Plain Tundra: Response to contrasting growing seasons. *Arctic Antarctic and Alpine Research* 43 (2):256–66.

Oren, R., C. I. Hsieh, P. Stoy, J. Albertson, H. R. McCarthy, P. A. Harrell, and G. G. Katul. 2006. Estimating the uncertainty in annual net ecosystem carbon exchange: Spatial variation in turbulent fluxes and sampling errors in eddy-covariance measurements. *Global Change Biology* 12 (5):883–96.

Pearcy, R. W., J. R. Ehleringer, H. A. Mooney, and P. W. Rundel. 1990. *Plant physiological ecology: Field methods and instrumentation*. London: Chapman and Hall.

Ping, C., J. Bockheim, J. Kimble, G. Michaelson, and D. Walker. 1998. Characteristics of cryogenic soils along a latitudinal transect in Arctic Alaska. *Journal of Geophysical Research* 103 (D22):28917–28928.

Raz-Yaseef, N., E. Rotenberg, and D. Yakir. 2010. Effects of spatial variations in soil evaporation caused by tree shading on water flux partitioning in a semi-arid pine forest. *Agricultural and Forest Meteorology* 150 (3):454–62.

Raz-Yaseef, N., J. M. Young-Robertson, T. Rahn, V. L. Sloan, B. D. Newman, C. Wilson, S. Wullschleger, and M. S. Torn. 2017. Evapotranspiration across plant types and geomorphological units in polygonal arctic tundra. *Journal of Hydrology* 553:816–25.

Sturm, M., C. Racine, and K. Tape. 2001. Climate change: Increasing shrub abundance in the Arctic. *Nature* 411 (6837):546–47.

Tape, K., M. Sturm, and C. Racine. 2006. The evidence for shrub expansion in Northern Alaska and the Pan-Arctic. *Global Change Biology* 12 (4):686–702.

Tenhunen, J., O. Lange, S. Hahn, R. Siegwolf, and S. Oberbauer. 1992. The ecosystem role of poikilohydric tundra plants. In *Arctic ecosystems in a changing climate*, ed. F. S. Chapin III, R. L. Jefferies, J. F. Reynolds, G. Shaver, A. J. Svoboda, and E. W. Chu, 213–37. San Diego, CA: Academic Press.

Valentini, R., S. Dore, G. Marchi, D. Mollicone, M. Panfyorov, C. Rebmann, O. Kolle, and E. D. Schulze. 2000. Carbon and water exchanges of two contrasting central Siberia landscape types: Regenerating forest and bog. *Functional Ecology* 14 (1):87–96.

Vourlitis, G. L., and W. C. Oechel. 1997. Landscape-scale CO_2, H_2O vapour and energy flux of moist-wet coastal tundra ecosystems over two growing seasons. *Journal of Ecology* 85 (5):575–90.

Wielgolaski, F., L. Bliss, J. Svoboda, and G. Doyle. 1981. Primary production of tundra. In *Tundra ecosystems: A comparative analysis*, ed. L. C. Bliss, O. W. Heal, and J. J. Moore, 187–226. Cambridge: Cambridge University Press.

Wullschleger, S. D., H. E. Epstein, E. O. Box, E. S. Euskirchen, S. Goswami, C. M. Iversen, J. Kattge, R. J. Norby, P. M. van Bodegom, and X. Xu. 2014. Plant functional types in Earth system models: Past experiences and future directions for application of dynamic vegetation models in high-latitude ecosystems. *Annals of Botany* 114 (1):1–16.

Wullschleger, S. D., F. C. Meinzer, and R. A. Vertessy. 1998. A review of whole-plant water use studies in trees. *Tree Physiology* 18 (8–9):499–512.